Supplementary Materials for

Rapid Progression of Ocean Acidification in the California Current System

Nicolas Gruber,* Claudine Hauri, Zouhair Lachkar, Damian Loher, Thomas L. Frölicher, Gian-Kasper Plattner

*To whom correspondence should be addressed. E-mail: nicolas.gruber@env.ethz.ch

Published 14 June 2012 on *Science* Express
DOI: 10.1126/science.1216773

This PDF file includes:

Model setup We set up the UCLA-ETH Version of the Regional Oceanic Modeling System (ROMS) for the entire California CS from the U.S./Canadian Border (48°N; approximately coincident with the subtropical/subpolar gyre boundary) to the latitude of the middle of Baja California (28°N), and extending out to about 1300 km from the shore. The standard setup has a horizontal resolution of 5 km and has 32 vertical levels, while we also developed a reduced resolution setup at 15 km for sensitivity analyses. A detailed description of the model setup used here is given in refs (*1*) and (*2*), including detailed comparisons with several in-situ and remotely sensed observations.

The standard model's high horizontal resolution as well as the fact that it uses a terrain-following (σ) coordinate system in the vertical permits the detailed modeling of the upwelling

processes occurring on and near the shallow shelf, which are crucial for determining the conditions in the nearshore environments of the California CS. A nitrogen-based nutrient-phytoplankton-zooplankton-detritus-type (NPZD) model was coupled to the physical setup, with the parameters chosen to reflect primarily the high-productivity regime in the nearshore areas (*3*). Thus, the simulations reported here use the same ecosystem parameters as ref (*2*), while ref (*1*) use a slightly altered set.

A carbon biogeochemistry module was added, representing the cycling of inorganic and organic carbon through the ecosystem, as well as the exchange of CO_2 across the air-sea interface. The carbon fluxes driven by the production and subsequent transformation of organic matter are tied to those of nitrogen with fixed stoichiometric ratio of 117:16. The biogenic formation of mineral $CaCO_3$ is modeled by assuming that a fixed fraction of 7% of net primary production is undertaken by organisms that form $CaCO_3$ shells. Once formed, $CaCO_3$ is modeled to sink with a sinking velocity of 20 m day^{-1} and to dissolve with a constant first order rate of 0.0057 day^{-1}. Since only a negligible amount of the produced $CaCO_3$ dissolves in the euphotic zone, while about half of the organic carbon is being remineralized, the resulting inorganic-to-organic carbon export ratio is about 14%. This is larger than the global mean export ratio of about 7 to 10% (*4, 5*), but typical of mid-latitude regions. The exchange of CO_2 across the air-sea interface is formulated employing a classical bulk parameterization approach (*6*) with the gas transfer velocity depending on the square of the wind speed (*7*). Given the climatological forcing, the coefficients for steady winds was selected. A sinusoidal seasonal cycle in atmospheric pCO_2 is considered estimated on the basis of the observed marine boundary layer (MBL) reference for the mean latitude of the California CS (*8*). The sediment is modeled using a "bucket" approach, where all sinking material arriving at the sediment-water interface is added to the sediment box and is then subject to aerobic remineralization and dissolution with rates that are lower than those in the water column. No anaerobic processes are considered.

The models were initialized with observations corresponding to nominal years of 1750 (pre-industrial) and 1995, respectively, with temperature, salinity, and nutrient concentrations taken from the World Ocean Atlas 2005 (http://www.nodc.noaa.gov/OC5/WOA05/pr_woa05.html), and with the carbon parameters provided by data from the GLobal Ocean Data Analysis Project (GLODAP) (*9*) for pre-industrial and present-day conditions. A seasonal cycle was added to the lateral DIC boundary conditions using a monthly climatology of surface ocean $p\mathrm{CO}_2$ (*10*) and assuming constant salinity normalized alkalinity. Similarly, a seasonal cycle was added to the lateral boundary conditions for alkalinity, using an observationally-based parameterization of alkalinity with regard to sea-surface temperature and salinity (*11*). The seasonal cycles of DIC and alkalinity were propagated downward by assuming that its seasonal amplitude decreases at the same rate as the seasonal amplitude of temperature decreases. All models were spun-up for at least 10 years, which proves sufficient for such regional models (*3*).

Model simulations Three simulations were undertaken with the standard 5 km resolution setup: A time-slice simulation to establish the pre-industrial conditions (see also (*12*)), a transient simulation from 1995 through 2050 to investigate the potential future evolution of the ocean's carbonate system in the California CS and a control simulation over the same time period to establish the model's drift. This drift turned out to be very small, so that the reported results are based on the transient simulations only. The physical part of the model remained the same, i.e., irrespective of the different simulation periods, the model was forced at the surface with the same monthly climatologies of momentum and density fluxes computed from QuikSCAT and the Comprehensive Ocean-Atmosphere Data Set (COADS) data products, respectively. Also the lateral boundary conditions for temperature, salinity, nutrients, and circulation remained the same. In contrast, the lateral and surface boundary conditions for the carbon system evolved with time: For the pre-industrial time-slice simulation, atmospheric $p\mathrm{CO}_2$ was

prescribed at 280 ppm, and the lateral DIC boundary conditions were those provided by the pre-industrial DIC field of GLODAP. For the transient simulation, atmospheric $p\mathrm{CO}_2$ increased from 364 ppm in 1995 to 541 ppm in 2050 (*13*) following the SRES A2 emissions scenario (*14*). At the lateral boundaries, the DIC concentrations were prescribed to increase as well, with the increases taken from a global Earth-system model simulation that was forced with either the SRES A2 emissions scenario. More specifically, we used the present-day DIC field of GLODAP as a basis, and each year a DIC increment was added, determined from simulations with the NCAR CSM1.4-carbon model (*13*) and defined as the modeled DIC difference at each location between DIC at time t $\geq$ 1995 and in 1995. Alkalinity was assumed to remain unchanged as it is not directly affected by the oceanic uptake of CO_2 from the atmosphere. For the control simulation, the lateral and atmospheric boundary conditions remained the same as those provided for 1995.

Three additional transient simulations were performed with the 15 km setup in order to investigate the sensitivity of the results to the emission pathway: A control run with atmospheric CO_2 and the lateral boundary conditions fixed for 1995, and two simulations where atmospheric CO_2 and the lateral boundary conditions for DIC increased according to the SRES A2 and B1 emissions scenarios (*14*). In the latter (low CO_2 emission) scenario, atmospheric CO_2 increases "only" to 492 ppm by 2050.

Model Evaluation The distributions of sea-surface temperature (SST) and chlorophyll in the standard setup compare well with satellite-based products (correlation coefficients r of $>$0.99 for SST and $\sim$0.8 for chlorophyll for the whole domain) (*1, 2*). Also the simulated distributions of density, nutrients, and chlorophyll in the interior ocean compare overall favorably with in-situ observations.

However, a couple of shortcomings have been identified (see e.g., Figures S6 and S7 in

Ref (*1*) and Figures 1 - 3 in Ref (*2*)). First, the offshore-onshore gradients of many thermocline properties is somewhat too weak in the model, possibly reflecting a too weak wind stress curl in our forcing. Second, the thermocline waters in the nearshore 300 km tend to be a bit too cold and too fresh, possibly indicating a too strong contribution of waters of northerly origin. Third, nitrate concentrations are too low in the upwelling waters, likely contributing to the the model underestimating net primary production in comparison to calibrated satellite-based estimates (*15*). These biases are of relatively modest size, however, and we consider them not to have important ramification for the future evolution of ocean acidification.

More important is the evaluation of the model simulated saturation state Ω_{arag}. To this end, we use the observations gathered during the U.S. West Coast Cruise undertaken in the summer 2007 (*16*) (data available from the Carbon Dioxide Analysis and Information Center (CDIAC) http://cdiac.ornl.gov/oceans/Coastal/NACP_West.html) and computed Ω_{arag} in the same manner as done in our model. We sampled the model along the same sections for the same month, but using a random day.

Comparison of four offshore sections along the Central California region between $\sim$35 °N and $\sim$42 °N reveal that the model tends to capture the surface to depth and the onshore-offshore gradients well, but that the model tends to overestimate Ω_{arag} throughout the water column (Fig. S1). It also tends to underestimate the vertical gradient in Ω_{arag}. As a result of these biases, the modeled depth of the saturation horizon for aragonite, i.e. Ω_{arag}= 1, is overall too deep. In the nearshore areas, the depth bias amounts to between 50 and 100 m, whereas further offshore, the depth bias is somewhat smaller, i.e., generally around 50 m. These agreements and mean biases are considerably overprinted by a substantial amount of smaller-scale variability within and between the sections, much more so in the observations than in the model. This underestimation of variability in our model results is to a large degree a consequence of our using monthly climatological forcing. This wind forcing therefore does not capture the day-to-day variability

in atmospheric conditions, which is an important cause of the observed smaller scale variations in Ω_{arag}, especially short-term upwelling events such as captured along line 5.

The Taylor diagram in Fig. S2 depicts the agreements and disagreements between the simulated and observed distribution of Ω_{arag} in a more quantitative manner. In the upper 100 m, model simulated Ω_{arag} is well correlated with the observations (r=0.68), while the correlation decreases to 0.57 further below. At the same time, the modeled standard deviation in relation to that in the observations decreases substantially from a ratio of above 0.8 in the upper 100 m to less than 0.4 in the depth range from 100 to 250 m. The trend reverses further down in the water column, with a higher correlation (r = 0.75) and a ratio of standard deviations of nearly 1.5. These numbers differ little between whether the analysis is done just for the central California CS domain or for the entire area covered by the U.S. West Coast Cruise. Also shown in Fig. S2 are the mean biases (mean errors), which range between about +0.06 to +0.08 in the upper 100 m to +0.11 to +0.15 in the depth range from 100 to 250 m (positive values indicating that the model overestimates the observed Ω_{arag}).

The reasons underlying these biases in Ω_{arag} are likely manifold. One contribution may come from the biases in the thermocline properties with the colder and fresher water of northern origin having, on average, higher Ω_{arag} than those of southern origin, which contain a substantial signature from the Eastern Tropical North Pacific oxygen minimum zone (*17*). Another potential reason is our possibly overestimating the vertical export of $CaCO_3$, which adds too much alkalinity to the thermocline upon the dissolution of this exported mineral. A third reason is the limited representativeness of the observations, as these were taken during a period of exceptionally large upwelling, which cannot be captured by our climatologically forced model.

The positive bias of the model's simulated Ω_{arag} distribution implies that the volumetric census of a particular class of Ω_{arag} will also be biased, i.e., that too little volume will be simulated to be in the low Ω_{arag} classes and especially in the undersaturated class. We applied no bias cor-

rection to our model since we considered the observations from one single cruise as insufficient to arrive at a representative bias distribution. The impact of applying a constant reduction of 0.1 to the simulated Ω_{arag} for the volume census is shown in Fig. S3.

References and Notes

1. N. Gruber, *et al.*, *Nature Geoscience* (2011).

2. Z. Lachkar, N. Gruber, *Biogeosciences* **8**, 2961 (2011).

3. N. Gruber, *et al.*, *Deep Sea Res. I* **53**, 1483 (2006).

4. J. L. Sarmiento, *et al.*, *Global Biogeochem. Cycles* **16** (2002). 1107, doi:1029/2002GB001919.

5. X. Jin, N. Gruber, J. Dunne, R. A. Armstrong, J. L. Sarmiento, *Global Biogeochem. Cycles* (2006).

6. J. L. Sarmiento, N. Gruber, *Ocean Biogeochemical Dynamics* (Princeton University Press, Princeton, New Jersey, 2006).

7. R. Wanninkhof, *J. Geophys. Res.* **97**, 7373 (1992).

8. GLOBALVIEW-CO_2, Cooperative Atmospheric Data Integration Project - Carbon Dioxide, *Tech. rep.*, NOAA ESRL, Boulder, Colo. (2011). (also available via anonymous FTP to ftp.cmdl.noaa.gov, Path: ccg/co2/GLOBALVIEW).

9. R. M. Key, *et al.*, *Global Biogeochem. Cycles* **18** (2004).

10. T. Takahashi, *et al.*, *Deep Sea Res. II* (2009).

11. K. Lee, *et al.*, *Geophys. Res. Lett.* **33** (2006).

12. C. Hauri, *et al.*, *Oceanography* **22**, 60 (2009).

13. T. L. Frölicher, F. Joos, G.-K. Plattner, M. Steinacher, S. C. Doney, *Global Biogeochem. Cycles* **23** (2009).

14. N. Nakicenovic, *et al.*, *Special Report on Emissions Scenarios : a special report of Working Group III of the Intergovernmental Panel on Climate Change* (Cambridge University Press, New York, 2000).

15. M. Kahru, R. Kudela, M. Manzano-Sarabia, B. G. Mitchell, *J. Geophys. Res.* **114** (2009).

16. R. A. Feely, C. L. Sabine, M. Hernandez-Ayon, D. Ianson, B. Hales, *Science* **320**, 1490 (2008).

17. C. G. Castro, F. P. Chavez, C. A. Collins, *Global Biogeochem. Cycles* **15**, 819 (2001).

18. P. Tans, R. F. Keeling, Recent Mauna Loa Data, *electronic data*, NOAA ESRL, Scripps Institution of Oceanography, Boulder, CO, USA (2012). Http://www.esrl.noaa.gov/gmd/ccgg/trends/.

Figure captions

Fig. S1. Comparison of model simulated Ω_{arag} with in situ observations from the U.S. West Coast Cruise in 2007 (*16*). Shown are a series of offshore sections at $\sim$ 42°N (line 5, panels a and c)), at $\sim$38 °N (line 7, panels b and d), at $\sim$37 °N (line 8, panels e and g) and at $\sim$35°N (line 9, panels f and h). The model section was sampled at a random day in the same month and year as the observations.

Fig. S2. Taylor diagram of model simulated Ω_{arag} in comparison with in situ observations from the U.S. West Coast Cruise (*16*). Shown in the figure are the relative standard deviations between the model simulated properties and the observations as the radial distance from the origin, and the correlation between the model and the observations as the angle from the vertical. The model was sampled on a random day in the same month and year as the observations. The numbers in the legend are the mean error of the model relative to the observations with positive values indicating that the model overestimates Ω_{arag}.

Fig. S3. Temporal evolution of volumes with a particular range of Ω_{arag}in the case for the model simulated Ω_{arag} having been corrected by lowering it by 0.1. Plotted in white are the temporal evolution of selected Ω_{arag} classes for the original case shown in the Figure 2 in the main text.

Fig. S4. Simulated Seasonal evolution of Ω_{arag} in the nearshore 10 km in 2050. Shown is an alongshore section for the top 120 m from 30°N to 50°N.

Fig. S5. Temporal evolution of atmospheric $p\text{CO}_2$ for the two employed IPCC-SRES scenarios, i.e., A2 and B1. The atmospheric CO_2 was simulated by the Earth-system model NCAR CSM1.4-carbon in response to the respective emission scenarios (*14*). Also shown is the observed timeseries of atmospheric CO_2 for the Mauna Loa site (*18*), indicating that both model-based scenarios have a positive bias of about 5 ppm, which is equivalent to the atmospheric growth over about 2 to 3 years. This small positive bias is a result of the NCAR CSM1.4-

carbon model having simulated a smaller CO_2 uptake from the atmosphere than observed (*13*).

Fig. S6. Temporal evolution of volumes with a particular range of Ω_{arag} in the upper ocean (0-60 m) for the (a) A2 and (b) B1 scenarios. The plotted results are based on simulations with the 15 km resolution setup.

Fig. S7. As Figure 3 in the main text, but for the A2 and B1 scenarios and based on the results from the simulations with the 15 km resolution setup.

Fig. S8. Relationship between the changes in Ω_{arag} (panels a,b), in the dissolved CO_2 concentration (a, c), and in pH (b, c) between 1995 and 2050 for the nearshore 50 km of the entire California Current. Plotted are the monthly mean differences for the month of January across all depths from the 5 km resolution model and the A2 scenario.

Figures

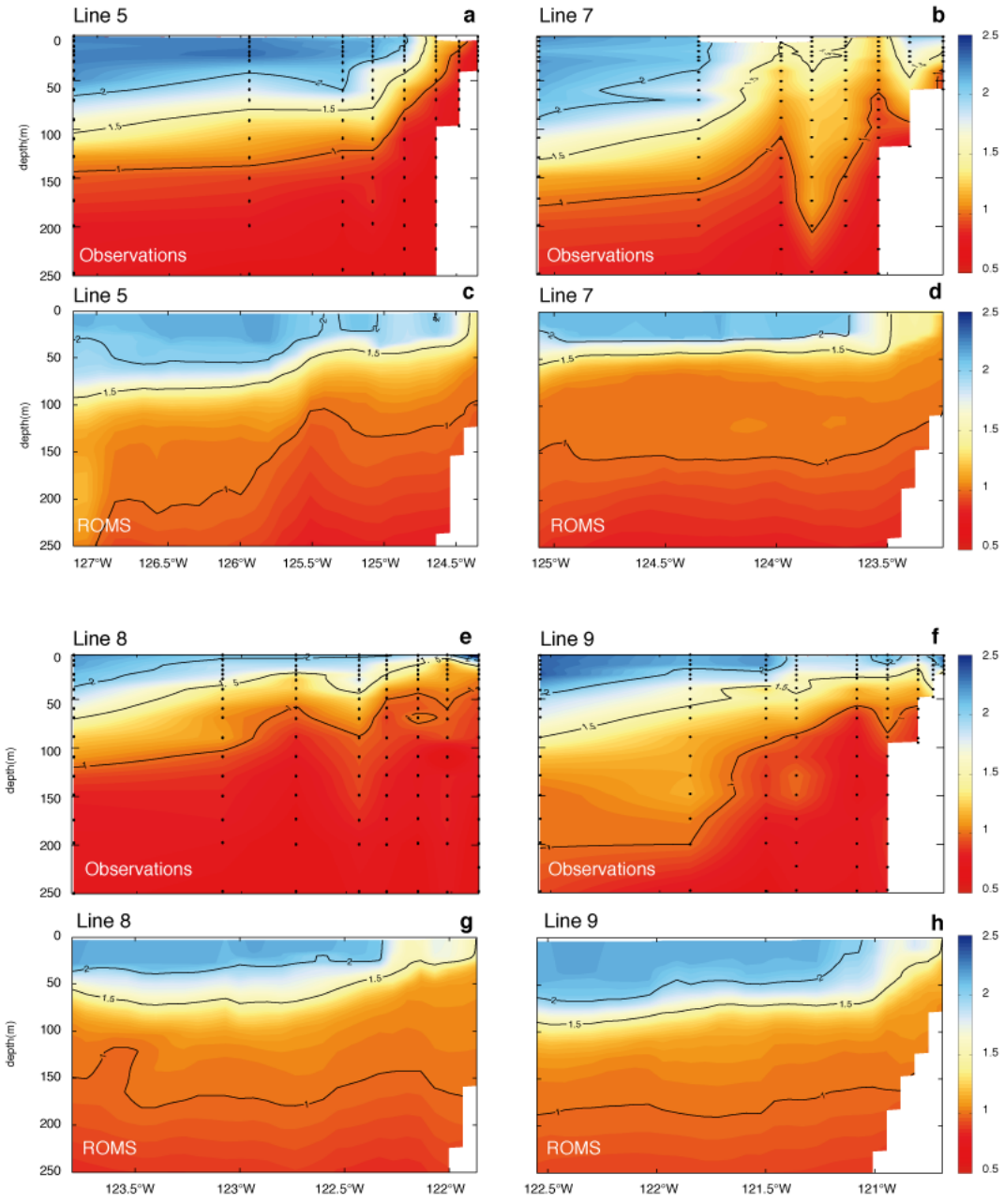
Line 5
a
Observations
Line 7
b
Observations
Line 5
c
ROMS
Line 7
d
ROMS
depth(m)
0
50
100
150
200
250
127°W
126.5°W
126°W
125.5°W
125°W
124.5°W
125°W
124.5°W
124°W
123.5°W
2.5
2
1.5
1
0.5
Line 8
e
Observations
Line 9
f
Observations
Line 8
g
ROMS
Line 9
h
ROMS
123.5°W
123°W
122.5°W
122°W
121.5°W
121°W

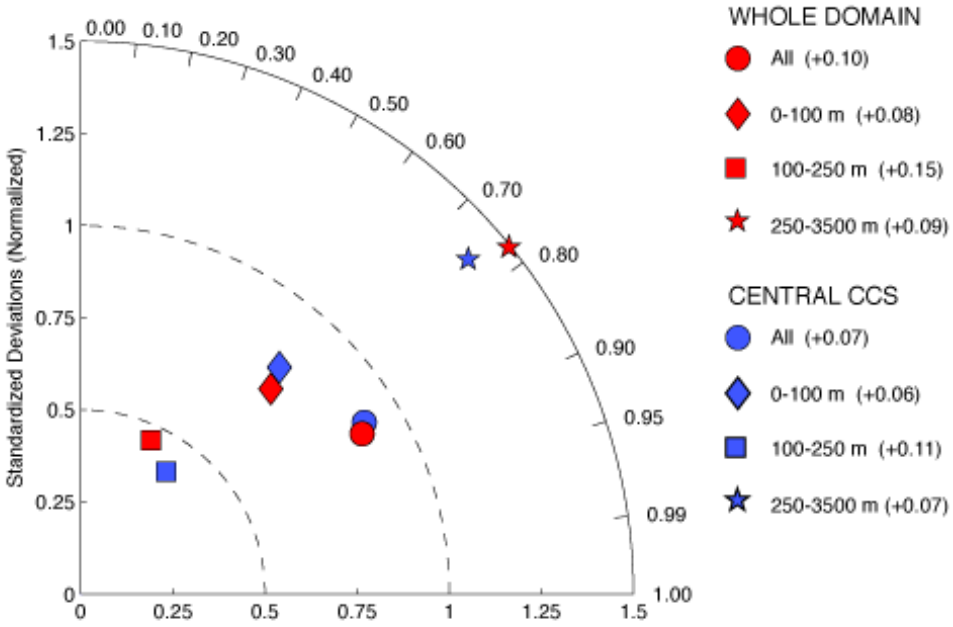
Standardized Deviations (Normalized)
0.00
0.10
0.20
0.30
0.40
0.50
0.60
0.70
0.80
0.90
0.95
0.99
1.00
0
0.25
0.5
0.75
1
1.25
1.5
WHOLE DOMAIN
All (+0.10)
0-100 m (+0.08)
100-250 m (+0.15)
250-3500 m (+0.09)
CENTRAL CCS
All (+0.07)
0-100 m (+0.06)
100-250 m (+0.11)
250-3500 m (+0.07)

Figure 2:

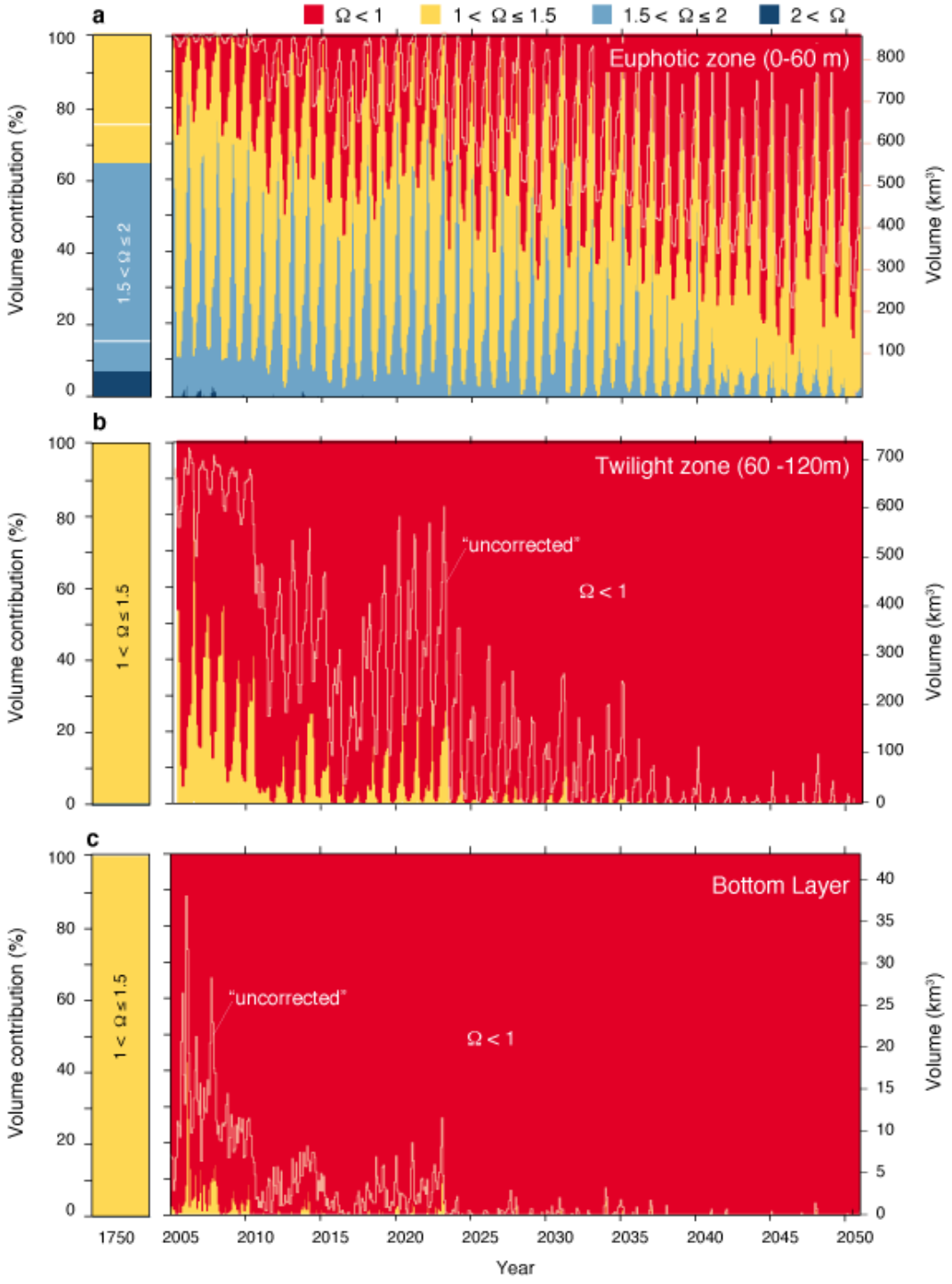
a
Ω < 1
1 < Ω ≤ 1.5
1.5 < Ω ≤ 2
2 < Ω
Euphotic zone (0-60 m)
Volume contribution (%)
Volume (km³)
1.5 < Ω ≤ 2
b
Twilight zone (60 -120m)
"uncorrected"
Ω < 1
1 < Ω ≤ 1.5
c
Bottom Layer
"uncorrected"
Ω < 1
1 < Ω ≤ 1.5
1750
2005
2010
2015
2020
2025
2030
2035
2040
2045
2050
Year

Figure 3:

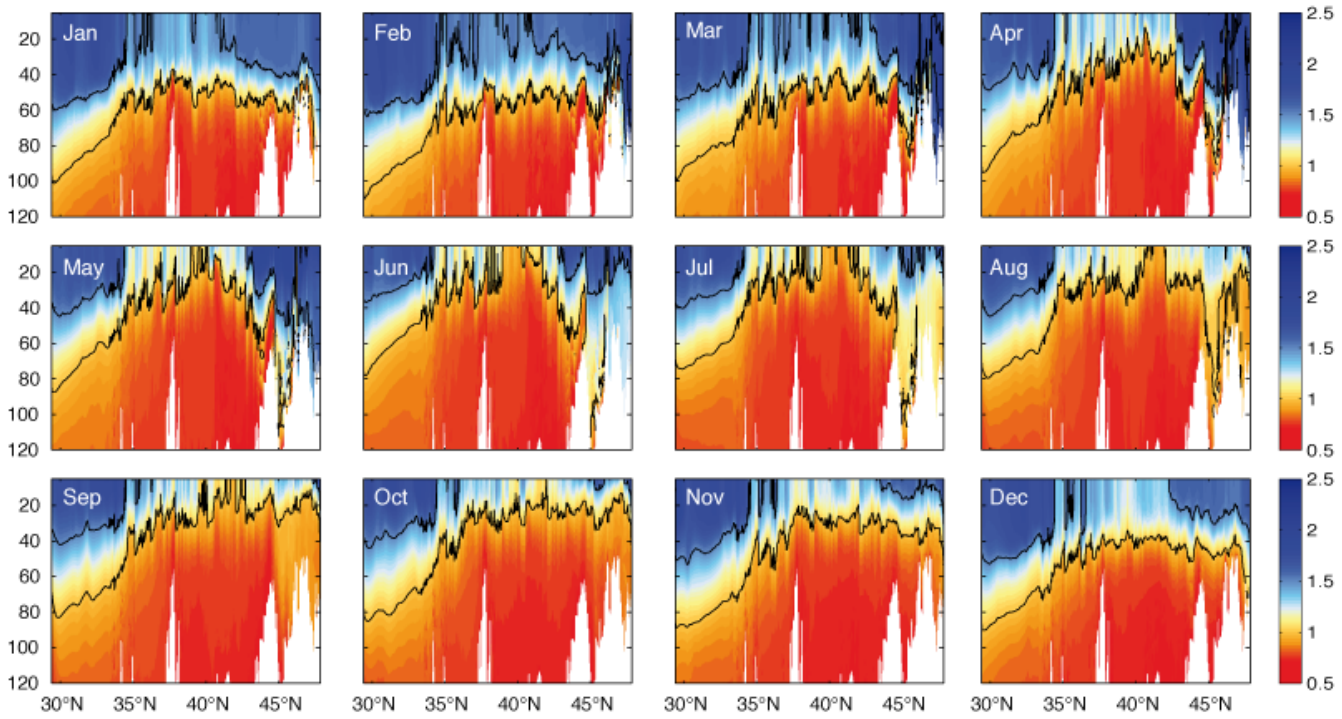

Figure 4:

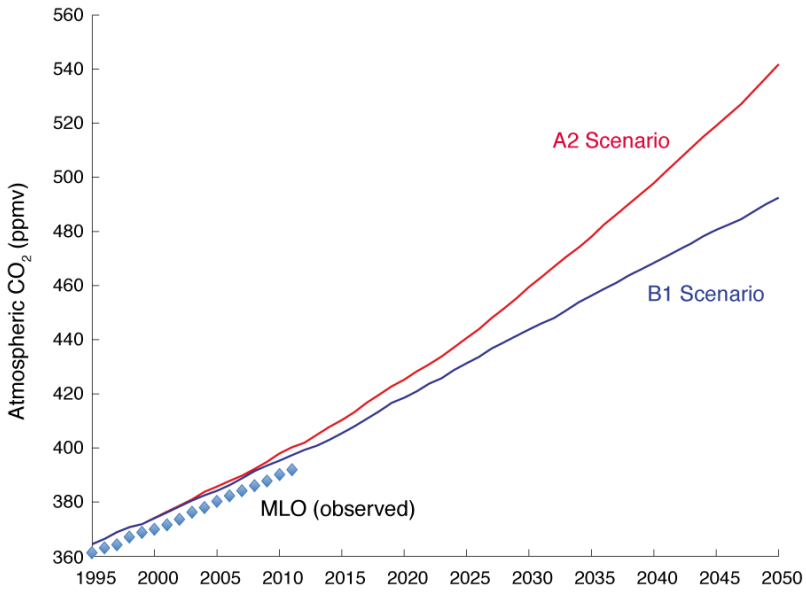

Figure 5:

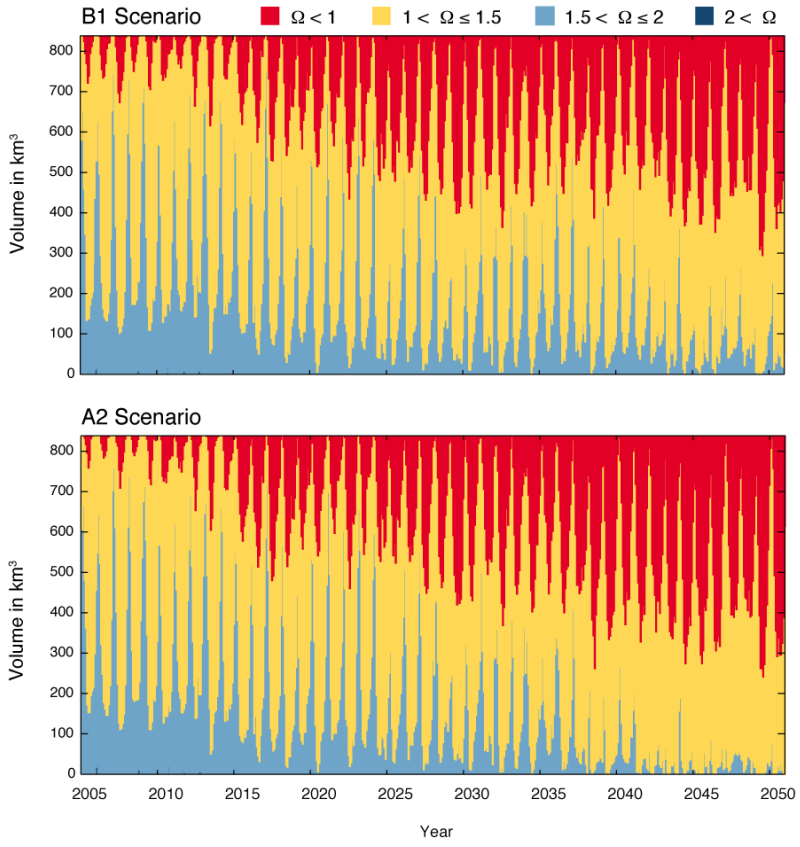
B1 Scenario
Ω < 1
1 < Ω ≤ 1.5
1.5 < Ω ≤ 2
2 < Ω
Volume in km³
800
700
600
500
400
300
200
100
0
A2 Scenario
Volume in km³
800
700
600
500
400
300
200
100
0
2005
2010
2015
2020
2025
2030
2035
2040
2045
2050
Year

Figure 6:

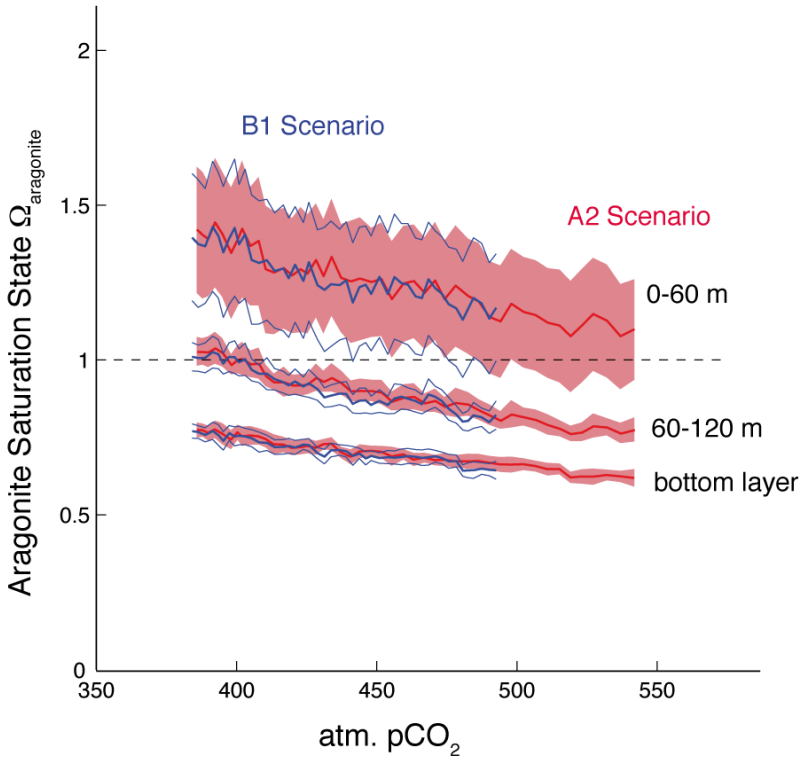

Figure 7:

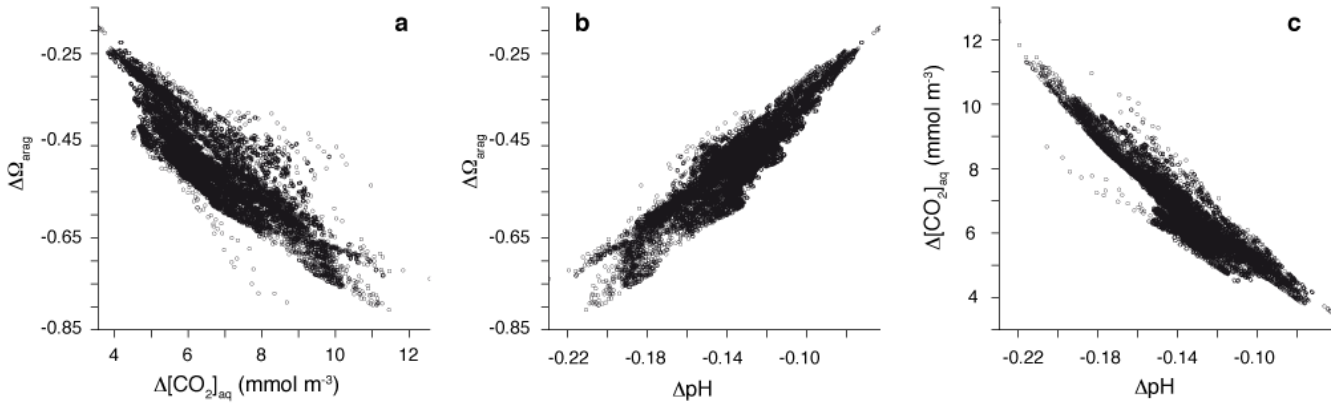

Figure 8: